Quantification of Cerebral Arterial Blood Volume Using Arterial Spin Labeling With Intravoxel Incoherent Motion-Sensitive Gradients

Tae Kim[1,3] and Seong-Gi Kim[1,2*]

Quantification of cerebral arterial blood volume (CBV_a) is important for understanding vascular regulation. To enable measurement of CBV_a with diffusion-weighted (DW) arterial spin labeling (ASL), a theoretical framework was developed using the effects of intravoxel incoherent motion (IVIM). The pseudo-diffusion coefficient (D^*) in the IVIM model was evaluated at 9.4 T in DW-ASL of rat brain under isoflurane anesthesia by variations of both post-labeling delay (w) and magnetization transfer ratio (MTR). D^* and its volume fraction decreased at values of $w \geq 0.3$ s, and the normalized apparent diffusion coefficient (ADC) increased with MTR, suggesting that D^* is closely correlated with CBV_a. Thus, the difference between ASL measurements with and without DW gradients is related to CBV_a. The CBV_a values measured by this approach were compared with values obtained using the modulation of tissue and vessel (MOTIVE) technique with ASL, which varies MT levels without changing spin labeling efficiency. CBV_a values from both methods were highly correlated. The measured CBV_a values were linearly correlated with cerebral blood flow (CBF) for a $PaCO_2$ range of 25–50 mmHg; ΔCBV_a (ml/100 g) = 0.007 (min^{-1}) × ΔCBF (ml/100 g/min). The DW-ASL approach is simple and easy to implement for human and animal CBV_a studies. Magn Reson Med 55:1047–1057, 2006. © 2006 Wiley-Liss, Inc.

Key words: cerebral arterial blood volume; arterial spin labeling; diffusion-weighted gradient; magnetization transfer; cerebral blood flow

Cerebral blood volume (CBV) has been measured by integrating MRI signals induced by the first-pass of contrast agents after bolus injection (1). Separation of CBV into arterial and venous volumes may provide further information regarding vascular regulation that is not obtainable from total CBV measurements. The quantification of arterial CBV (CBV_a) may therefore be useful for evaluating both normal cerebral function and pathology related to vascular disease. However, the CBV_a is a small fraction of the total brain volume, i.e. ~1% (2,3), and is therefore difficult to map. We recently developed an MRI method to determine CBV_a by *mo*dulation of *ti*ssue and *ve*ssel (MOTIVE) signals (2). This technique employs magnetization transfer (MT) (4,5) to selectively modulate tissue signals without changing arterial blood signals, while blood signal is modulated either by injection of a contrast agent or by arterial spin labeling (ASL). Arterial blood volume maps of rat brain were successfully obtained by utilizing two coils with this technique. However, when continuous ASL (CASL) is implemented with a single coil, the MT effect induced by the labeling pulses decreases brain tissue signal, and it is not trivial to modulate MT levels without changing ASL efficiency. Thus, it is desirable to find a way to measure CBV_a without having to modulate the MT level.

The contribution of arterial blood signals in ASL can be reduced by employing small magnetic field gradients (referred to in the literature as diffusion, Stejskal-Tanner, or bipolar gradients) that dephase the signal from rapidly flowing spins. This approach has been used to suppress signal contributions from larger arterial vessels (6). In perfusion studies this same property was implemented with multiple spin tagging times to attempt measurement of CBV_a (preliminary data were reported in abstract form (7–9)). By adapting the intravoxel incoherent motion (IVIM) approach (10) for use with CASL measurements, the component with fast apparent diffusion coefficient (ADC) can be separated from tissue spins with slow ADC (11). The fast ADC component has been considered to arise from "unextracted" labeled spins in capillaries and veins. Since disturbed and inhomogeneous flow of spins within arterial vessels can also be considered to be a pseudo-diffusive process, we hypothesize that arterial blood is the major source of the pseudo-diffusion component in ASL measurements with IVIM-sensitive gradients. Thus, if the signals suppressed by diffusion gradients originate from arterial vasculature, one can measure CBV_a by incorporating this diffusion gradient.

In this study we determined the source of the pseudo-diffusion component in IVIM with ASL measurements in rat brain by varying both the post-labeling delay time and the MT effect without changing the ASL efficiency. ASL experiments were performed with both the proposed diffusion-weighted (DW) method and the MOTIVE approach (no diffusion gradient) in the same animals to determine whether the independently measured CBV_a and CBF values were consistent. The relationship between CBV_a and CBF was also determined.

THEORY

Source of the Pseudo-Diffusion Component in IVIM With ASL Measurements

In ASL studies it is assumed that signal changes in an imaging voxel are due to contribution from three compart-

[1]Department of Radiology, University of Pittsburgh, Pittsburgh, Pennsylvania, USA.

[2]Department of Neurology, University of Pittsburgh, Pittsburgh, Pennsylvania, USA.

[3]Center for Magnetic Resonance Research, Department of Radiology, University of Minnesota, Minneapolis, Minnesota, USA.

Grant sponsor: NIH; Grant numbers: EE003375; EB003324; NS44589; EB001977.

*Correspondence to: Seong-Gi Kim, Ph.D., Department of Radiology, University of Pittsburgh Medical School, 3025 E. Carson St., Pittsburgh, PA 15203. E-mail: kimsg@ pitt.edu

Received 21 July 2005; revised 12 December 2005; accepted 6 January 2006.
DOI 10.1002/mrm.20867
Published online 4 April 2006 in Wiley InterScience (www.interscience.wiley.com).

ments: arterial blood, tissue/capillary, and venous blood. The loss of spin labeling due to T_1 relaxation during travel time minimizes contributions of labeled spins from venous blood. Further, T_2 of venous blood at 9.4 T is very short relative to T_2 of tissue and arterial blood (12). When the echo time (TE) is >3 times T_2 of venous blood in spin-echo data collection, signal from the venous pool becomes negligible. Therefore, the remaining signal arises from a combination of arterial blood and tissue/capillary contributions. When spin labeling time is >2 s, labeled water in capillaries freely exchanges with tissue water (the exchange time of water is ~500 ms (13)). Under these conditions, longitudinal magnetizations of tissue and capillary water are indistinguishable during the spin preparation period. In this application, tissue and capillary are treated as one compartment.

The difference between the "control" signal (without ASL) and "labeled" signal (with ASL) is given by $\Delta S_{sat} = S_{sat}^{control} - S_{sat}^{label}$, where the subscripts refer to some degree of macromolecular saturation in tissue by the MT-inducing pulses. In our descriptions, $S_{sat}^{control}$ is used interchangeably with S_{sat}. When ASL pulses are applied in the absence of MT effects (as in the two-coil setup), $S_{sat}^{control} = S_0$ and $\Delta S_{sat} = \Delta S_0$, where the subscript zero indicates no MT saturation. If we assume that D^* arises from arterial spins, when DW gradients are applied ΔS_{sat} with MT saturation at TE, $\Delta S_{sat}(b)$, is described as

$$\Delta S_{sat}(b) = (1 - \nu_a) \cdot \Delta M_{sat}^{tissue} \cdot e^{-b \cdot D} \cdot e^{-TE \cdot R_{2(tissue)}} + \nu_a \cdot \Delta M_0^{artery} \cdot e^{-b \cdot D^*} \cdot e^{-TE \cdot R_{2(artery)}}, \quad [1]$$

where ν_a is the fraction of arterial spins; ΔM_{sat}^{tissue} and ΔM_0^{artery} are changes in magnetization induced by CASL in tissue in the presence of MT, and in arterial blood in the absence of MT, respectively; $R_{2(\text{tissue})}$ and $R_{2(\text{artery})}$ are the $1/T_2$ values of tissue and arterial blood water, respectively; D is the water diffusion coefficient in the tissue/capillary pool; and D^* is the pseudo-diffusion coefficient in the arterial pool. Assuming rectangular-shaped gradient pulses, the diffusion factor, b (in a unit of sec/mm^2), can be expressed as $b = (\gamma \cdot \delta \cdot G)^2(\Delta - \delta/3)$, where γ is the gyromagnetic ratio of proton nuclei, δ is the duration of each gradient, G is the DW gradient strength, and Δ is the time between gradient onsets (14).

$\Delta S_{sat}(b)$ normalized to conditions under MT saturation but without DW gradients (ΔS_{sat} (0)) is determined as

$$\Delta S_{sat}(b)/\Delta S_{sat}(0) = (1 - f) \cdot e^{-b \cdot D} + f \cdot e^{-b \cdot D^*} = e^{-b \cdot ADC}, \quad [2]$$

where the volume fraction of the pseudo-diffusion coefficient (f) is equal to $\nu_a \cdot \Delta M_0^{artery} \cdot e^{-R_{2(artery)} \cdot TE}/((1 - \nu_a) \cdot \Delta M_{sat}^{tissue} \cdot e^{-R_{2(tissue)} \cdot TE} + \nu_a \cdot \Delta M_0^{artery} \cdot e^{-R_{2(artery)} \cdot TE})$. According to simulation, f is linearly correlated to ν_a within the ν_a range of 0.5–2%. At 9.4 T, T_2 of tissue and arterial blood is similar (12), and therefore T_2 differences can be ignored in Eq. [1].

To evaluate whether the pseudo-diffusion coefficient component (D^*) is indeed related to arterial blood volume, as we propose here, diffusion measurements with ASL can be executed with variable post-labeling delay times (w). Spins tagged at the labeling plane travel along arterial blood vessels and first enter the imaging plane at τ_a. The spins reach the capillaries at τ_c, where they then exchange with tissue water (Fig. 1). With incorporation of w, the relative signal contribution of the arterial blood pool to $\Delta S_{sat}(b)$ will then be dependent on w, τ_a, and τ_c. The arterial blood volume contribution will be partially reduced when $\tau_a < w < \tau_c$, and totally eliminated when $w > \tau_c$ (Fig. 1). If our model is correct, $\Delta S_{sat}(b)/\Delta S_{sat}(0)$ will follow a biexponential decay when $w < \tau_c$ (i.e. there will still be pseudo-diffusion contributions from arterial blood), and a single-exponential decay when $w > \tau_c$. Also, the calculated ADC value will progressively decrease when $\tau_a < w < \tau_c$ because the D^* contribution decreases.

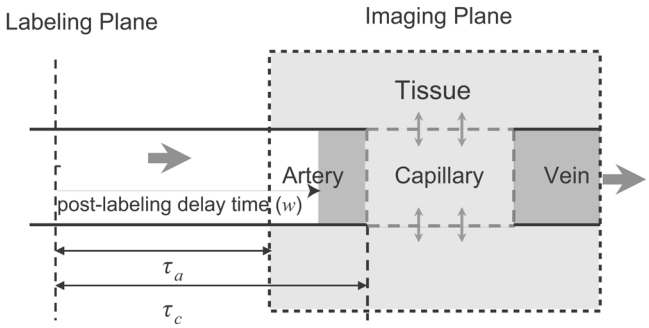

FIG. 1. Schematic of blood delivery from labeling plane to various compartments within the imaging plane, which consists of arteries, tissue/capillary, and veins. At the capillary level the labeled water exchanges with tissue water. τ_a: Transit time from labeling plane to entry of the imaging plane. τ_c: Transit time from labeling plane to the exchange site. Postlabeling delay (w) allows fresh spins, which are unlabeled, to enter arterial vasculature. The contribution of arterial blood volume to ΔS data will therefore be partially reduced when $\tau_a < w < \tau_c$, and totally eliminated when $w > \tau_c$.

In CASL studies employing one homogeneous head coil, MT effects induced by long spin labeling RF pulse(s) will be unavoidable in the tissue/capillary pool (15,16) but leave arterial blood signals unaffected. One can also examine the pseudo-diffusion coefficient by exploiting these MT effects. If arterial blood is a major contribution to D^*, then the relative contribution of arterial blood to ΔS_{sat} will be greater when tissue signal is reduced by increasing the MT effects without changing spin labeling efficiency. If our model is correct, calculated ADC values will increase with MT saturation level because the relative contribution from D^* increases.

Determination of Arterial Blood Volume From ASL Data With DW Gradients

When the arterial blood contribution is removed by an appropriate DW gradient (e.g., b = 100 s/mm^2), only the tissue/capillary pool remains. The DW-ASL data can be normalized as

$$\Delta S_{sat}(b)/S_0(b) = \Delta M_{sat}^{tissue}/M_0^{tissue}, \quad [3]$$

where $S_0(b)$ is the signal intensity of control images at the same b-value without any MT effect, and M_0^{tissue} is the

tissue magnetization in the absence of MT and ASL. When arterial signals are removed, normalized ΔS_{sat} is independent of MT level and post-labeling delay. However, when no DW gradient is applied ($b = 0$), the arterial component remains in ΔS_{sat}, and normalization can then be obtained with

$$\Delta S_{sat}(0)/S_0(0) \cong [(1 - \nu_a) \cdot \Delta M_{sat}^{tissue} + \nu_a \cdot \Delta M_0^{artery} \cdot \xi]/M_0^{tissue}, \quad [4]$$

where $\xi = e^{-(R_{2(artery)} - R_{2(tissue)}) \cdot TE}$ and $S_0(0) \cong M_0^{tissue} \cdot e^{-R_{s(tissue)} \cdot TE}$. By definition, $\Delta M_0^{artery} = 2\alpha_a \cdot M_0$, where α_a is the labeling efficiency of arterial spins in the imaging slice (17); α_a is reduced due to T_1 relaxation during travel from the labeling plane, such that $\alpha_a = \alpha_o \cdot e^{-(\tau_a \cdot R_{1b})}$, where α_o is the degree of labeling efficiency at the labeling plane, and R_{1b} is $1/T_1$ of arterial blood. The $\Delta M_{sat}^{tissue}/M_0^{tissue}$ term in Eq. [4] can be replaced by the equivalence in Eq. [3] to yield the fraction of arterial spins as

$$\nu_a = \frac{[\Delta S_{sat}(0)/S_0(0)] - [\Delta S_{sat}(b)/S_0(b)]}{2\alpha_a \cdot \xi - [\Delta S_{sat}(b)/S_0(b)]}. \quad [5]$$

When ASL pulses induce MT effects (as in the case of single-coil ASL), $S_0(b)$ and $S_0(0)$ must be determined without MT effects in separate acquisitions. However, when ASL pulses do not induce MT effects (as for two-coil ASL), then it is not necessary to obtain $S_0(b)$ and $S_0(0)$ from separate acquisitions, as these values would be directly obtainable from the control signals.

From data acquired with multiple MT saturation levels without applying DW gradients and without changing arterial labeling efficiency, a fraction of arterial blood spins can also be calculated by the MOTIVE method (2). In short, the normalized ASL data, $\Delta S_{sat}/S_0$ can be written as

$$\Delta S_{sat}/S_0 = C \cdot (S_{sat}/S_0) + \nu_a(2\alpha_a - C) \cdot \xi, \quad [6]$$

where C is related to tissue/capillary perfusion; $C = \frac{\Delta M_{sat}^{tissue}}{M_{sat}^{tissue}} = \left(2\alpha \cdot \frac{CBF}{\lambda}\right) \Big/ \left(\frac{1}{T_1} + \frac{CBF}{\lambda}\right)$ (18,19), T_1 is T_1 of tissue without MT effects, and λ is the blood to brain partition coefficient. The venous contribution to S_{sat} can also be ignored if both tissue and venous spins experience the same degree of saturation by MT. By fitting a linear function to $\Delta S_{sat}/S_0$ vs. S_{sat}/S_0, a slope (C) and intercept ($\nu_a \cdot (2\alpha_a - \text{slope}) \cdot \xi$) are obtained. The arterial spin fraction is thus

$$\nu_a = \frac{Intercept}{(2\alpha_a - C) \cdot \xi}. \quad [7]$$

Since C is much less than $2\alpha_a$, the slope term can be ignored in quantification of ν_a. At 9.4 T, the ξ term in Eqs. [4]–[7]) is one because the T_2 values of arterial blood and tissue are similar, and therefore the ξ term was not included in calculations in this study and previous reports (2). However, the ξ term can be significant at low magnetic fields (see Discussion).

It should be noted that the spin density of tissue is different from that of blood. However, ν_a is the fraction of spins in the arterial blood pool (units of %), which incorporates this difference of spin density, and thus a change in spin density will be reflected in ν_a values. In order to convert from spin fraction (ν_a) into physical volume (CBV_a), differences in spin density between tissue and blood pools have to be considered. Thus, CBV_a will be $\nu_a \times \lambda$ where λ is the blood to brain partition coefficient (ml blood/g tissue).

MATERIALS AND METHODS

Animal Preparation

The animal protocols used in this study were approved by the University of Pittsburgh Animal Care and Use Committee. Eighteen male Sprague-Dawley rats weighing 350–450 g (Charles River Laboratories, Wilmington, MA, USA) were initially anesthetized with 5% isoflurane in a 1:2 mixture of O_2:N_2O gases and intubated for mechanical ventilation (RSP-1002; Kent Scientific, CT, USA). The isoflurane level was reduced to 2% for surgical preparation. During MR experiments the O_2:N_2O mixture was replaced with air maintaining ~30% O_2, and isoflurane levels were reduced to ~1.5%. The femoral artery was catheterized for blood pressure monitoring and blood gas sampling, and the femoral vein was catheterized for fluid administration. The arterial blood pressure and breathing pattern were recorded with a multi-trace unit (AcKnowledge; Biopak, CA, USA) during the experiments. Ventilation rate and volume were adjusted based on blood gas analysis results (Stat profile pHOx; Nova Biomedical, MA, USA). Before it was placed in the magnet the head of the animal was carefully secured in an in-house-built restrainer by means of ear pieces and a bite bar to reduce head motion. The animal's rectal temperature was maintained at 37°C ± 0.5°C with a warm-water pad, a rectal thermal coupled probe, and a feedback unit.

MRI Methods

All MRI measurements were performed on a 9.4 Tesla magnet with bore diameter of 31 cm, interfaced to a Unity INOVA console (Varian, Palo Alto, CA, USA). The gradient coil was an actively shielded 12-cm inner diameter set with a gradient strength of 40 G/cm and a rise time of 130 μs (Magnex, Abingdon, UK). Two actively detunable RF coils were used: a butterfly-shaped surface coil was positioned in the neck region for ASL, while a surface coil of 2.3 cm diameter was positioned on top of the rat head both for tissue saturation via MT effects and for image acquisition (2). The homogeneity of the magnetic field was manually optimized on a slab that was twice as thick as the imaging slice.

A single 2-mm-thick coronal slice was selected. All images were acquired using an adiabatic single-shot double spin echo-planar imaging (EPI) sequence (12) with TE = 36 ms, TR = 10 s, matrix size = 64 (readout) × 32 (phase-encode), and FOV = 3.0 (right–left hemisphere direction) × 1.5 (dorsal–ventral direction) cm^2. B_1-insensitive flip angles were obtained by using a non-slice-selective adiabatic half passage (AHP) RF pulse for spin excitation,

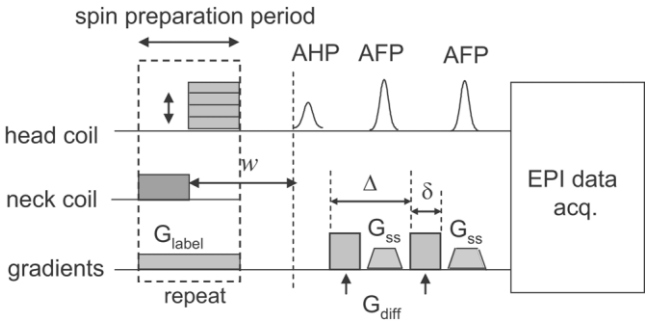

FIG. 2. Pulse sequence for ASL with DW gradients utilizing two actively detunable coils. A neck coil labels arterial spins with 100-ms pulses, while a head coil generates MT effects with 100-ms pulses. The spin preparation period (8 s) consists of consecutive repetition of this pair of pulses in the presence of a labeling gradient (G_{label}) along the *z*-axis (10 mT/m). To generate different MT saturation levels, the RF power level for MT pulses is adjusted without changing spin labeling efficiency. The delay following the final ASL pulses in the spin preparation (*w*) is variable. The head coil is also utilized for image acquisition by single-shot, double spin-echo EPI. A non-slice-selective AHF pulse provides spin excitation, and two slice-selective AFP pulses refocus spins in the presence of a slice-selection gradient (G_{ss}) on the *z*-axis. Both adiabatic pulses are based on sech amplitude and tanh frequency modulation functions. Diffusion-sensitizing unipolar gradients (G_{diff}) are applied around the first AFP pulse simultaneously along the *x*-, *y*-, and *z*-axes.

and two slice-selective adiabatic full passage (AFP) RF refocusing pulses for compensation of nonlinear phase (20). Diffusion-sensitizing unipolar gradients were applied around the first 180° RF pulse, with $\Delta = 20$ ms and $\Delta = 3$ ms (Fig. 2). Gradient strength was adjusted to achieve the desired *b*-value.

To control the level of MT effects without changing ASL efficiency, a pair of pulses consisting of a 100-ms spin tagging pulse in the neck coil followed by a 100-ms MT-inducing pulse in the head coil was repeated during 8 s of the spin preparation period (Fig. 2). The targeted MT saturation level in tissue was achieved by adjusting the power level of MT-inducing RF pulses with +8500 Hz off-resonance frequency using the head coil. The signal saturated by MT effects is described by the MT ratio (MTR), which is quantitatively $1 - (S_{sat}/S_0)$. To obtain signal changes induced by ASL, control and spin-labeled images were obtained in an interleaved manner with an applied field gradient strength of 1 gauss/cm. The labeling frequency was −8500 Hz, and the control frequency was +8500 Hz with respect to the resonance frequency.

Simultaneous Change of Post-labeling Delay Time and DW Gradients in ASL

To examine the characteristics of IVIM in ASL data, both DW gradient strength and post-labeling delay time were varied in 10 animals under normocapnic conditions. A post-labeling delay time (*w*) was inserted after the final spin labeling pulse in the spin preparation period to allow fresh unlabeled spins to enter the arterial vasculature within the imaging plane (Fig. 2) (21). Two separate animal groups were used in order to limit data acquisition to a reasonable experimental time. In five animals, the values for *w* were 0.1, 0.2, 0.3, 0.4 and 0.5 s, and the *b*-values were 0, 4, 11, 22, 32, 53, 104, and 155 s/mm^2. In another five animals, *w*-values were 0.1, 0.3, 0.5 and 0.7 s, and *b*-values were 0, 4, 11, 22, 32, 53, 74, 104, and 206 s/mm^2. Calculation of *b*-values took into account a cross-term from the imaging gradient (22). The order of the *w*- and *b*-values was randomized. To enhance the relative contribution of arterial blood to ASL data, tissue signal was partially suppressed by the MT effect (MTR = 0.56 ± 0.06, $N = 10$).

Variation of MT Levels With and Without DW Gradients

Eight animals were examined by ASL measurements without a post-labeling delay. Ventilation rate and volume were changed to adjust the $PaCO_2$ level. ASL was performed by modulation of MTR at target values of 0, 0.2, 0.4, and 0.6 in randomized order without any DW gradient ($b = 0$), and this modulation of MTR levels was then repeated with inclusion of a DW gradient ($b = 104$ s/mm^2). The purpose of these experiments was to calculate ADC values as a function of MTR for determining the signal source of the fast ADC component, and compare CBV_a values determined by the DW gradient approach (e.g., Eq. [5]), with those obtained by the MOTIVE method (e.g., Eq. [7]).

Data Processing

To improve the signal-to-noise ratio (SNR), 15–20 measurements were repeated for each condition and averaged before further analysis. Based on anatomic images, areas containing cerebral spinal fluid (CSF) were identified because the diffusion coefficient of CSF is larger than that of tissue (23). Regions of interest (ROIs) were then defined to include all of the brain within the slice, but with the exclusion of CSF.

Simultaneous Change of Postlabeling Delay Time and DW Gradients in ASL

Normalized signals with DW gradients at each post-labeling delay time were fitted using a biexponential nonlinear least-square method (ORIGIN 7.0; Microcal, Northampton, MA, USA) according to Eq. [2]. To compare with biexponential fitting, ADC values for $\Delta S_{sat}(b)/\Delta S_{sat}(0)$ and $S_{sat}(b)/S_{sat}(0)$ data were also determined at each post-labeling delay time by single-exponential linear fitting.

ADC Calculation With Variation of MT Levels

ADC values were determined from data acquired with *b*-values of 0 and 104 s/mm^2. For each of the four MTR values, ADC was calculated by $-\ln(\Delta S_{sat}(b)/\Delta S_{sat}(0))/b$, where $b = 104$. To remove intersubject variations, the resulting four ADC values from each animal were normalized to the ADC value obtained with MTR = 0. To compare with experimental data, the normalized ADC value was also simulated at different MTR levels assuming D^* arises from arterial component with the following parameters; $\Delta M_{sat}^{tissue} = (1 - MTR)\Delta M_0^{tissue}$, where $\Delta M_0^{tissue} = 0.043$ (CBF = 2 ml/g/min), $\Delta M_0{}^{artery} = 2 \cdot \alpha_a \cdot M_0 = 0.72$, $D = 0.8 \times 10^{-3}$ and 1.2×10^{-3} mm^2/s, $D^* = 40 \times 10^{-3}$ and 400×10^{-3} mm^2/s, and $\nu_a = 0.005$ and 0.015 using

$$\Delta S_{sat}(b)/\Delta S_{sat}(0) = [(1 - \nu_a) \cdot \Delta M_{sat}^{tissue} \cdot e^{-b \cdot D} + \nu_a \cdot \Delta M_0^{artery} \cdot e^{-bD^*}]/[(1 - \nu_a) \cdot \Delta M_{sat}^{tissue} + \nu_a \cdot \Delta M_0^{artery}]. \quad [8]$$

CBV_a and CBF Calculations With Variation of MT Levels

$\Delta S_{sat}(b)/S_{sat}(b)$ and $\Delta S_{sat}(0)/S_{sat}(0)$ were plotted as a function of MTR to determine whether the *b*-value employed (104 s/mm^2) was sufficient to eliminate arterial blood signals. Then arterial blood spin fractions were determined for each $PaCO_2$ level in each animal by two approaches: 1) four ν_a values were calculated from each pair of data with and without DW gradients obtained at four MTR values using Eq. [5], and 2) one ν_a value was determined from the subset of this same data without DW gradients by Eq. [7], which is equivalent to the MOTIVE approach ($\alpha_a = 0.36$ was used in both calculations according to our previous measurements with the same setup and parameters (2)). CBV_a was then determined as $\nu_a \times 0.9$ (ml blood/g tissue) (24).

CBF without contribution from arterial blood vessels was examined with both the DW approach and the MOTIVE method. For the DW approach, four CBF values from each MTR with the application of diffusion gradients were calculated using a conventional single-compartment model as

$$CBF = \frac{\lambda}{T_1}\left(\frac{\Delta S_{sat}}{2\alpha \cdot S_{sat} - \Delta S_{sat}}\right) \quad [9]$$

where T_1 is measured from tissue without MT effect, α is the spin tagging efficiency, and S_{sat} is the signal intensity of the control image at each MT level. We assumed that $\lambda = 0.9$ ml/g and $T_1 = 2$ s (2). Since the arterial blood volume contribution is suppressed by a *b*-value of 104 s/mm^2, the spin tagging efficiency is determined by the T_1 relaxation of labeled spins during travel from the labeling plane to the exchange site in the capillaries; $\alpha = \alpha_c$, which is $\alpha_o \cdot e^{-(\tau_c \cdot R_{1b})}$. The value for α was determined in our previous measurements ($\alpha_o = 0.41$, $\tau_c = 0.6$ s, and $R_{1b} = 0.435$ s^{-1} (2)). For the MOTIVE method, CBF was calculated from the subset of data acquired with multiple MTR values without DW gradients by $CBF = \frac{\lambda}{T_1}\left(\frac{C}{2\alpha_c - C}\right)$ where *C* is the slope of a fitted line of the MT-dependent data as a function of normalized baseline signal (see Eq. [6]) (2).

CBF and CBV_a values obtained by both methods were compared. Statistical analyses were performed using one-way analysis of variance (ANOVA) and *t*-test for the criterion of statistical significance. Data in the text are reported as the mean ± standard deviation (SD).

RESULTS

Simultaneous Changes of Postlabeling Delay Time and DW Gradients in ASL

To determine whether the *D** component in the IVIM model is related to arterial blood, $\Delta S_{sat}(b)/\Delta S_{sat}(0)$ was fitted to a biexponential function for each post-labeling delay (*w*) in each of 10 animals, and coefficients of fast (*D**) and slow (*D*) diffusion components and their fractions (*f* and 1 - *f,* respectively) were determined. Although there appeared to be a slight decline in *D* values at $w = 0.5$ and 0.7 (Fig. 3a), there was no statistical difference in *D* values as a function of *w* (one-way ANOVA, $F(5,39) = 2.38$, $P > 0.05$), which suggests that this component represents the tissue pool. On the other hand, *D** and its volume fraction (*f*) decrease as *w* increases, indicating that the pseudo-diffusion component is closely correlated to *w*. These effects can be explained if *D** represents the arterial blood volume contribution: an increase in *w* allows fresh spins to fill the arterial blood volume within the imaging slice, reducing the contribution of arterial blood to ΔS_{sat}. Previous rat studies (17,25) have shown that *w*-values of 0.1 and 0.2 s do not affect ΔS_{sat}, because these times are shorter

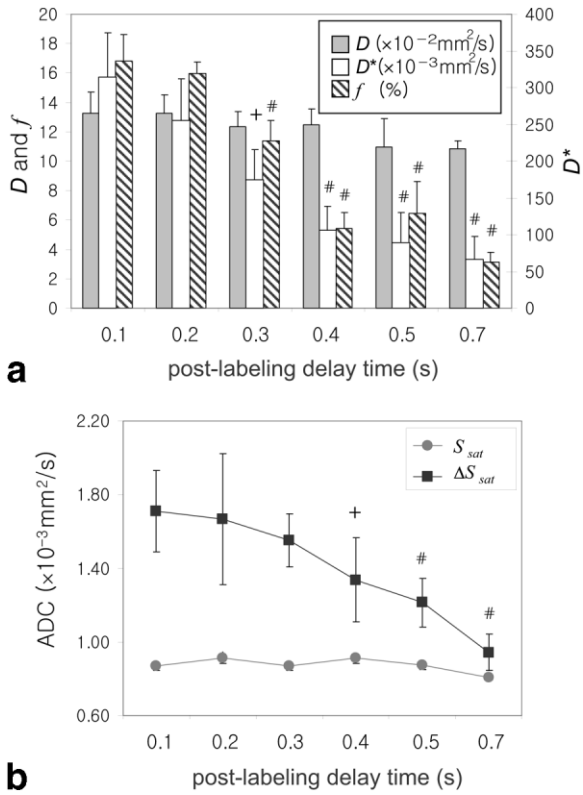

FIG. 3. Effect of post-labeling delay on diffusion values. **a:** The fast-moving ADC component (*D**), slow ADC component (*D*), and the fraction of *D** (*f*) are plotted as a function of post-labeling delay (*w*). $\Delta S_{sat}(b)/\Delta S_{sat}(0)$ obtained within the ROI was fitted to a biexponential function for each value of *w*; *D** and *f* decrease with *w*, while *D* is invariant of *w*. It should be noted that *D* and *D** units are different by a factor of 10. **b:** Single exponential ADC values calculated from ΔS_{sat} decrease with increasing *w*, while ADC values calculated from S_{sat} (unlabeled data) are invariant of *w*. Decreased ADC values in ΔS_{sat} can be explained by a decrease in the arterial volume contribution with the increase in *w*. All acquisitions were performed with an MTR value of ~0.56 for partial suppression of tissue signal. Data with $w = 0.1$, 0.3, and 0.5: $N = 10$; data with $w = 0.2$, 0.4, and 0.7: $N = 5$. Pound marks (#) indicate that the difference from data acquired with $w = 0.1$ s is statistically highly significant (*t*-test, $P < 0.01$). The plus mark (+) indicates that the same difference yielded $P < 0.05$. Error bars: SEM.

than the transit time from the labeling plane to imaging slice. In the current studies the differences between f values obtained with $w = 0.1$ s and data with $w \geq 0.3$ s were statistically highly significant (t-test, $P < 0.01$: pound mark (#) in Fig. 3a), and the differences between D^* values for the same comparisons were also statistically significant ($P < 0.05$: plus mark (+); $P < 0.01$; pound mark (#) in Fig. 3a). This could indicate that the transit time from labeling plane to imaging plane (τ_a) is less than 0.4 s. Even though accurate determination of D^* can be problematic due to the limited data points, the general w-dependent characteristic of D^* is consistent across all 10 animals, and indicates that D^* does represent the arterial blood contribution to ASL. Although data were combined from two different groups, the behaviors of D, D^*, and f in both individual groups were similar.

ADC values in ASL derived from single exponential fitting decreased with an increase in post-labeling delay ($F(5,39) = 7.35$, $P < 0.01$), as shown in Fig. 3b. The differences between ADC values acquired from data with $w = 0.1$ s and data with $w \geq 0.4$ s were statistically significant (t-test, $P < 0.05$: plus mark (+); $P < 0.01$: pound mark (#) in Fig. 3b). Decreased ADC values in ΔS_{sat} at longer w can be explained by the decreased contribution of arterial blood, and, as expected, ADC values of S_{sat} (control data) are independent of w ($F(5,39) = 1.55$, $P > 0.05$). ADC values of ASL with $w \leq 0.5$ s were significantly higher than ADC values of corresponding control data ($P < 0.005$, paired t-test), but ADC values of ASL with $w = 0.7$ s were not significantly different from those of control data ($P > 0.1$, paired t-test), suggesting that the arterial blood contribution is minimal at $w = 0.7$ s. This observation is consistent with the assumption that the fast pseudo-diffusion component in ASL is related to arterial blood signals. CBF values without and with removal of CBV_a contribution were 259 ± 61 ml/100 g/min and 229 ± 48 ml/100 g/min, respectively.

ADC Measurement With Variation of MT Levels

To further determine the source of the pseudo-diffusion component in ASL signals, normalized ADC values (ADC with MT saturation ($= -\ln(\Delta S_{sat}(b)/\Delta S_{sat}(0))/b$) divided by ADC without MT saturation) were computed, where b-values were 0 and 104 s/mm^2 and MTR values were 0, 0.24 ± 0.009, 0.40 ± 0.01, and 0.61 ± 0.006 ($N = 12$). At each MT level, data points from all 12 studies were averaged. Normalized ADC of S_{sat} appears to be independent of MTR (filled squares in Fig. 4) because the relative contribution of arterial blood to control signal is relatively small (i.e., 0.5–1.5% without MT effects and 1–4% with MTR of 0.56). However, the normalized ADC value of ΔS_{sat} increases with MTR (filled circles in Fig. 4). This can be explained by the fact that saturation of tissue signal induced by the MT effect increases the relative contribution of arterial blood to ΔS_{sat} (15–30% with MTR of 0.56); as MTR increases, the contribution of the D^* component is accentuated. Simulations performed to show normalized ADC values of ΔS_{sat} at each of eight different MT levels for varying D, D^*, and v_a, are also plotted in Fig. 4 (unfilled, ×, and + symbols). These simulated ADC values with v_a values of 0.5–1.5% match very well with the experimental data, suggesting that our model can explain the DW-ASL results at varied MTR.

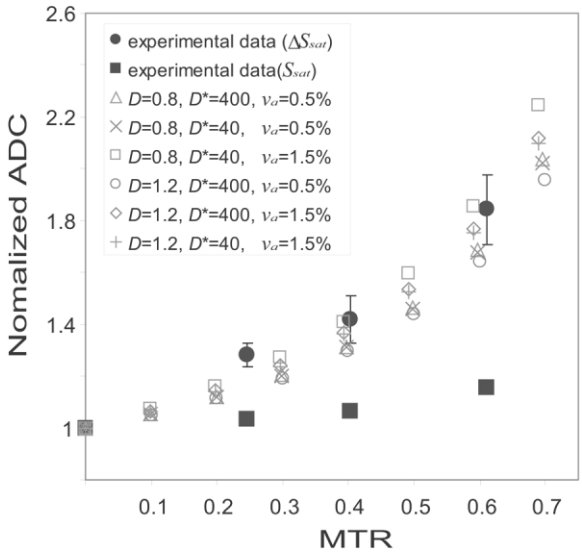

FIG. 4. ADC vs. MTR. ADC values were determined from data at two values of b for each MTR level. The normalized ADC value of ΔS_{sat} increased with MTR as shown by filled circles, while normalized ADC of S_{sat} was almost independent of MTR (filled squares). This can be explained by the fact that saturation of tissue signal induced by the MT effect increases the relative contribution of arterial blood to ΔS_{sat}; as MTR increases, the contribution of D^* component is accentuated. Also, simulations were performed at eight different MTR values for varying D, D^*, and v_a. Values for D and D^* indicated in legend are in units of 10^{-3} mm^2/s. Error bars: SEM. Most error bars are not visible, due to extremely small variations. The simulated ADC values match very well with the experimental data.

Measurement of CBV_a and CBF

To confirm that a b-value of 104 s/mm^2 is sufficient to remove the arterial blood volume contribution, normalized ASL data were plotted as a function of MTR in Fig. 5 for b-values of 0 and 104 s/mm^2. Twelve studies in eight animals were performed with $PaCO_2$ values of 25–50 mmHg. When no DW gradient was used, $\Delta S_{sat}(0)/S_{sat}(0)$ increased as MTR increased (solid lines in Fig. 5), in agreement with our previous findings (2). Data with no MT effect were statistically different from data for each nonzero MTR (t-test, $P < 0.01$). However, with a b-value of 104 s/mm^2, $\Delta S_{sat}(b)/S_{sat}(b)$ was independent of MTR (dotted lines in Fig. 5; $F(3,44) = 0.01$, $P > 0.05$). Therefore, the arterial volume contribution is removed to a level below the detection limit when $b = 104$ s/mm^2. When the arterial blood contributions are insignificant, normalized ASL signal is directly related to CBF.

Since the measured CBV_a values cannot be independently confirmed due to the lack of a gold standard method, we compared CBV_a values measured by two different MR approaches to determine consistency. Figure 6a shows CBV_a values calculated at each of four MTR values using the DW gradient method (Eq. [5]) with $b = 0$ and 104 s/mm^2 in each of 12 studies, compared with the single CBV_a value obtained using the MOTIVE approach (Eq. [7])

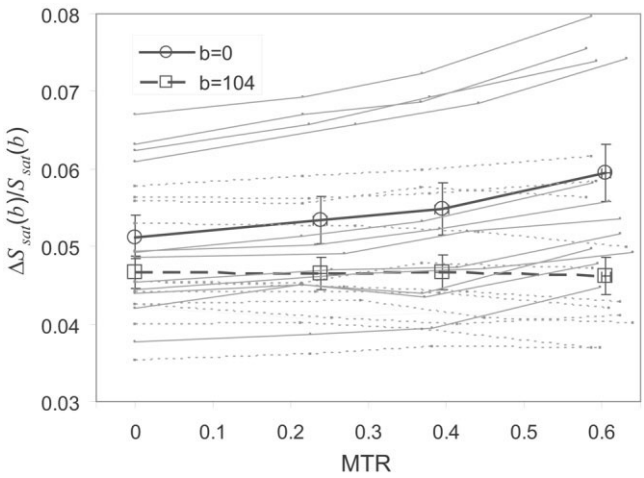

FIG. 5. ASL data at four different MTR values. Each light gray line (solid lines: b = 0 s/mm^2; dotted lines: b = 104 s/mm^2) represents an individual study (N = 12). $PaCO_2$ was intentionally elevated in four studies. When no DW gradient was applied, ΔS_{sat} (b = 0)/S_{sat} (b = 0) increased as MTR increased because the progressive saturation of tissue left a relatively higher arterial blood volume contribution (circles with black solid line; mean ± SEM). With the application of a sufficiently strong DW gradient, ΔS_{sat} (b = 104)/S_{sat} (b = 104) became independent of MTR, which can be explained by removal of the arterial volume contribution to a level below the detection limit (squares with black dashed line; mean ± SEM).

in each study. In the DW data, CBV_a values obtained with large MT saturation appear slightly higher than values obtained from without MT. However, CBV_a values obtained from the DW gradient method at each MT level were not significantly different from the single values determined by the MOTIVE method ($P > 0.05$). Thus, when the arterial blood component is removed by a sufficient b-value, CBV_a can be determined from data irrespective of MT level, and CBV_a maps of rat brain were therefore successfully obtained from data averaged for all four MTR values in order to enhance SNR. CBV_a maps obtained with both the DW method and the MOTIVE technique were very similar (examples in Fig. 6c and d, respectively).

CBF values without an arterial blood contribution were also determined with the DW method using the conventional single-compartment model with b = 104 s/mm^2, and with the MOTIVE approach using linear fitting to the tissue signal dependence on MT. Calculated CBF values also were highly correlated between the DW method and the MOTIVE method (R^2 = 0.98 for MTR = 0; R^2 = 0.96 for MTR = 0.24; R^2 = 0.91 for MTR = 0.40; R^2 = 0.91 for MTR = 0.61).

To compare CBV_a and CBF obtained from the DW method, values for each of the four MT levels were averaged. In measurements by both the DW method and the MOTIVE approach (Fig. 7), CBV_a and CBF values were

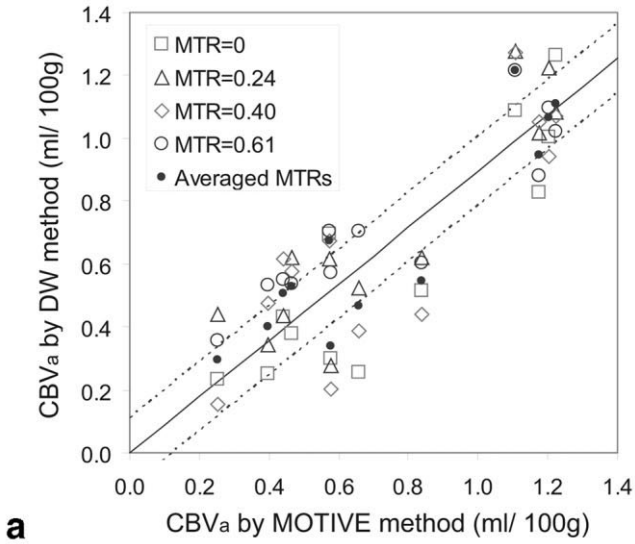

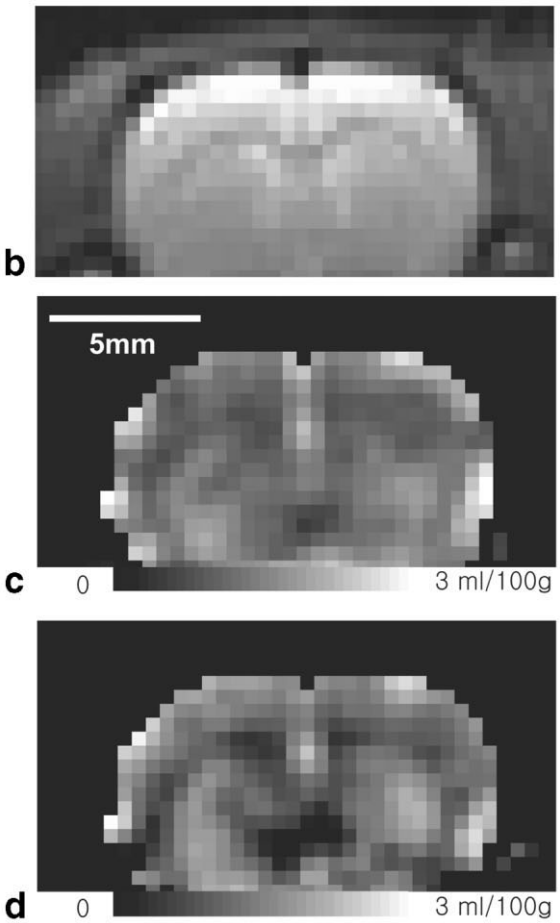

FIG. 6. Comparison of CBV_a values calculated from data acquired with a DW vs. the MOTIVE technique without the DW gradient. **a:** CBV_a values computed for four different MTR values from the DW gradient method (Eq. [5]) vs. MOTIVE (Eq. [7]; N = 12). CBV_a values obtained from the MOTIVE method were highly correlated with those from the diffusion gradient method (R^2 = 0.79 for MTR = 0; R^2 = 0.81 for MTR = 0.24; R^2 = 0.68 for MTR = 0.40; R^2 = 0.83 for MTR = 0.61). Solid line is fit to all MTR data and dotted lines are the averaged SD from fitted line (SD was calculated from data from each of four MTR values minus mean value (shown as filled circles)). **b:** The echo-planar image is shown for anatomical reference. Arterial blood volume maps are examples obtained from one animal by the (**c**) DW and (**d**) MOTIVE techniques.

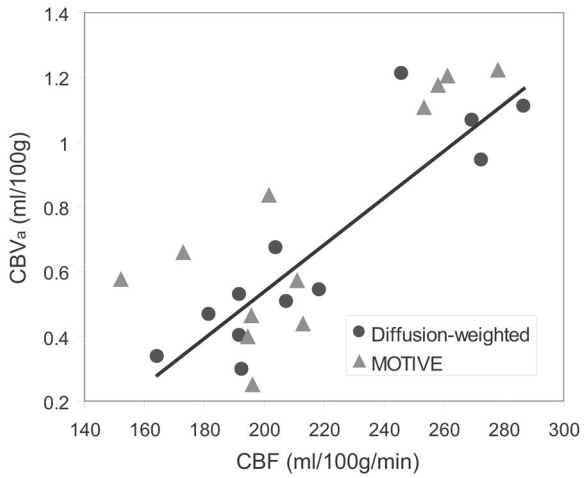

FIG. 7. Dependence of CBV_a on CBF values using the DW gradient (circles) and MOTIVE (triangles) techniques for all studies. For data obtained with the DW method, values for each of four MTRs were averaged for each of the 12 studies. The best-fitted lines are also shown. CBV_a is linearly correlated with CBF within the range of our studies; ΔCBF (ml/100 g/min) = 0.007(min^{-1}) · ΔCBV_a (ml/100 g). According to the central volume principle, the time between entry of arterial labeled spins in the imaging slice and their exchange with tissue ($\tau_c - \tau_a$) is 0.007 min (= 0.4 s).

linearly correlated within the $PaCO_2$ range of our studies (25–50 mmHg); CBV_a (ml/100 g) = 0.0072 (min^{-1}) × CBF (ml/100 g/min) − 0.91 (ml/100 g) (R^2 = 0.80) with the diffusion gradient method (circles in Fig. 7), and CBV_a (ml/100 g) = 0.0073 (min^{-1}) × CBF (ml/100 g/min) − 0.82 (ml/100 g) (R^2 = 0.64) with the MOTIVE method (triangles in Fig. 7). The higher correlation between CBF and CBV_a in DW vs. MOTIVE approaches may be due to the limited number of studies and slightly different assumptions used, and/or the differences in amount of data acquired for the two methods. CBV_a was calculated in the DW method from data with and without diffusion gradients, while CBV_a calculations by MOTIVE included only the data without diffusion gradients.

DISCUSSION

Consideration of the Capillary Component in the Model

Since the venous blood volume contributions to ASL measurements are negligible at 9.4 T, blood volume measured by the DW gradient approach in ASL studies is assumed to represent arterial blood volume. When ASL is achieved at a steady-state condition, the change in longitudinal magnetization of tissue/capillary is $\Delta M_{sat} = C \cdot M_{sat}$, where C is related to tissue perfusion (see Theory). However, the diffusion coefficients of tissue and capillary water are different, and thus when TE is much shorter than the exchange time of water, their transverse magnetization components are separable. Therefore, the tissue and capillary components can be modeled independently and, ignoring T_2 components, Eq. [1] can be rewritten as

$$\Delta S_{sat}(b) = [(1 - \nu_c - \nu_a) \cdot C \cdot M_{sat} \cdot e^{-b \cdot D} + \nu_c \cdot C \cdot M_{sat} \cdot e^{-b \cdot D_c^*} + \nu_a \cdot 2\alpha_a \cdot M_0 \cdot e^{-b \cdot D_a^*}], \quad [10]$$

where ν_c and ν_a are the capillary and arterial spin fractions, respectively; D is the diffusion coefficient of tissue; and D_c^* and D_a^* are the pseudo-diffusion coefficients of capillary and arterial blood, respectively. To determine the significance of the capillary contribution to ADC values, simulations were performed for $-\ln(\Delta S_{sat}(b)/\Delta S_{sat}(0))/b$, where b = 104 s/mm^2 with varying MTR using Eq. [10]. Parameters common to all simulations are CBF = 200 ml/100 g/min (C = 0.043), $D = 1.0 \times 10^{-3}$ mm^2/s, $D_a^* = 400 \times 10^{-3}$ mm^2/s, α_a = 0.36, and b = 0 and 104 s/mm^2. Results are shown in Fig. 8 with the assumption of no MT effects in arterial signal for the following conditions: 1) no capillary signal contributions to ΔS_{sat} (ν_c = 0%, ν_a = 1%) (diamonds); 2) longitudinal magnetization in capillaries is reduced by the MT effect to the same degree as tissue (ν_c = 1%, ν_a = 1%) (triangles), with $D_c^* = 20 \times 10^{-3}$ mm^2/s (26); and 3) no arterial signal contributes to ΔS_{sat}, and longitudinal magnetization in capillaries is reduced by the MT effect to the same degree as tissue (ν_c = 1%, ν_a = 0%) (squares), with $D_c^* = 20 \times 10^{-3}$ mm^2/s. Simulation results assuming arterial contributions (conditions 1 and 2 show similar dependencies of normalized ADC values on MTR, and closely match the experimental data. However, the simulation results assuming no arterial contribution are independent of MTR. This suggests that with these simulation parameters the capillary component does not contribute to a measurable increase in ADC values calculated as a function of MTR; rather, the arterial component is the

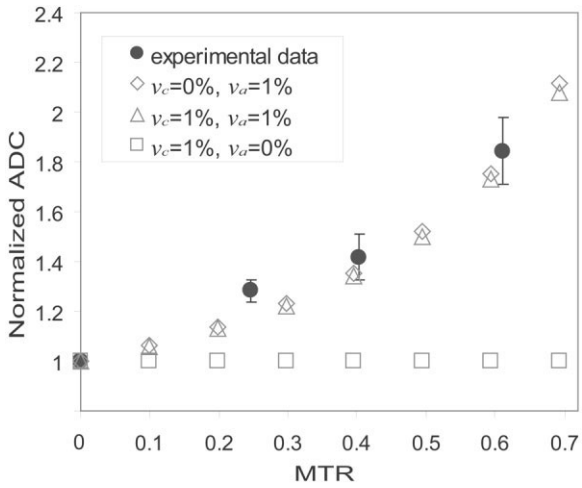

FIG. 8. Simulated ADC values using Eq. [10] for different capillary and arterial contributions vs. MT level. Parameters common to all simulations are CBF = 200 ml/100 g/min, $D = 1.0 \times 10^{-3}$$mm^2$/s, D_a^* = 400 × 10^{-3} mm^2/s, α_a = 0.36, and b = 0 and 104 s/mm^2. Three different conditions were simulated with the assumption of no MT effect in arterial signal: 1) no capillary signal contribution to ΔS_{sat} (diamonds); 2) capillary signals are reduced by the MT effect to the same degree as tissue with $D_c^* = 20 \times 10^{-3}$ mm^2/s (triangles); and 3) no arterial contribution to ΔS_{sat}, and capillary signals are reduced by the MT effect to the same degree as tissue with $D_c^* = 20 \times 10^{-3}$ mm^2/s (squares). With simulations including arterial contributions (conditions 1 and 2), normalized ADC values increase similarly with MTR and match the experimental data. However, under the assumption of no arterial signal contribution, normalized ADC is independent of MTR. This shows that the capillary component is not a major factor contributing to the increase in ADC with MTR.

dominant factor for this increase. Thus we conclude that arterial blood is the main contributor to the pseudo-diffusion component in ASL. However, if our assumption in the theory is not correct (i.e., if the labeled spins in capillaries do not completely exchange with tissue spins), then our measured CBV_a values are overestimated due to unextracted capillary spins, whose contribution is removed by DW gradients.

Evaluation of IVIM Measurements

Our data support the notion that the fast D^* component in ASL studies originates from the arterial blood compartment. When the tissue contribution is decreased by the MT effect, the fraction of the D^* component (i.e., f) increases. Also, the fraction of the D^* component is closely dependent on post-labeling delay time in our studies, which is another indication that D^* originates from arterial blood. Our data are consistent with IVIM measurements in ASL by Silva et al. at 4.7 T (11), where $D = 1.3 \times 10^{-3}$ mm^2/s, $D^* = 407 \times 10^{-3}$ mm^2/s, and the fraction of the D^* component (f) = 15% at CBF levels of 145 ml/100 g/min with MTR ~0.7 (11). Our closest comparison data at 9.4 T show that $D = \sim 1.3 \times 10^{-3}$ mm^2/s, $D^* = \sim 280 \times 10^{-3}$ mm^2/s, and f = 16–17% at a CBF level of 260 ml/100 g/min with MTR = ~0.56 and with b = 0 s/mm^2 and 0.1–0.2 s post-labeling delay (without removal of the arterial volume contribution). These different CBF values measured under similar physiological conditions may be due to the different anesthesia conditions used (2.5% halothane anesthesia in Silva et al. vs. 1.5% isoflurane here). The measured volume fraction of D^* is also affected by the different transverse relaxation rates of tissue and blood, as shown by the term ξ in Eqs. [4] and [5]. Without consideration of this contribution at 4.7 T, at TE = 47 ms with arterial blood and tissue T_2 values of 83 ms (27) and 67 ms (28), respectively, the measured ν_a is ~13% overestimated. Even so, D^* and its volume fraction in our measurement agree reasonably well with those reported by Silva et al. However, our interpretation of the D^* component differs from that of Silva et al. (arterial spins in the present study vs. unextracted spins in both veins and capillaries in Silva et al.). The increasing fraction of the D^* component at higher CBF levels reported by Silva et al. can also be explained by higher CBV_a at higher CBF levels, as shown in Fig. 7.

Arterial Blood Volume Measurements With ASL Methods

Arterial blood volume can be determined by separating the arterial blood signals from the tissue signals in ASL measurements. This can be achieved by either selective reduction of the tissue signals by MT saturation, or by removal of arterial blood signals using DW gradients. Both approaches yield consistent CBV_a values. Our measured CBV_a values of ~0.7 ml/100 g (Fig. 6a) agree well with previously measured values of 1.0 ml/100 g obtained by the MOTIVE method with ASL at five MT saturation levels (at a CBF level of ~200 ml/100 g/min) (2). Since the fraction of arterial blood volume is ~30% of the total blood volume at CBF of ~100 ml/100 g/min (see Fig. 6 in Ref. 12), the total blood volume in this study is estimated to be ~2.3% of total volume, which is within the reported values of ~2–5% in rats (29–31).

The calculation of ν_a is highly dependent on accurate determination of spin labeling efficiency (α_a) because both $\Delta S_{sat}(b)/S_0(b)$ and slope (C) are small relative to $2 \cdot \alpha_a$, as shown in Eqs. [5] and [7], respectively. Thus, the exact evaluation of transit time to imaging plane, which is not trivial for measurement, is important for calculation of α_a. We used an apparent transit time of τ_a = 0.3 s. However, the actual transit time will be between τ_a and τ_c. If the actual transit time = 0.45 s, then our measured ν_a would be overestimated by 7%.

CBV_a can also be measured using the central volume principle with values for CBF and the transit time of arterial blood. Transit time was evaluated by Wang et al. (32) in conjunction with ASL with a diffusion gradient and post-labeling delay time in the range of τ_a–τ_c. According to their method, when the duration of the labeling pulse is long, with an appropriate diffusion gradient, $\Delta S_0(b)/S_0(b) = k \exp(-\tau_c \cdot R_{1b})$ and without a diffusion gradient, $\Delta S_0(0)/S_0(0) = k \exp(-w \cdot R_{1b})$, where k is $\frac{2 \cdot f \cdot \alpha_0}{\lambda \cdot R_1}$. From data with and without DW gradients, the transit time from the labeling plane to capillary can therefore be determined as $\tau_c = -\ln\left(\frac{\Delta S_0(b)/S_0(b)}{\Delta S_0(0)/S_0(0)} \cdot e^{-w \cdot R_{1b}}\right)/R_{1b}$. In our studies with w = 0.4 and 0.5 s (shown in Fig. 3), this quantification of τ_c yields 0.64 ± 0.10 s (15 measurements in 10 animals). In this data set, τ_a appears to be ~0.3 s, and CBF = ~230 ml/100 g/min (with removal of CBV_a contribution). Thus, $CBV_a = CBF \times (\tau_c - \tau_a)$ = ~3.8 ml/100 g/s × (0.6 s − 0.3 s) = 1.14 ml/100 g, which is consistent with our previous results (2) and our current findings.

Comparison of the DW and MOTIVE Methods

Since both the MOTIVE and DW methods can be implemented to determine CBV_a from ASL measurements, it is important to critically evaluate the properties of both methods. Although the arterial blood volume fraction is on the order of 1% of total brain volume, quantitative CBV_a values were robustly measured because in ASL studies the ratio of signal originating from arterial blood relative to tissue is much greater than the actual arterial blood volume fraction. In our studies, signals originating from arterial blood were typically 10–15% of ΔS_0. If the tissue signal is further suppressed by MT effects, the relative contribution of arterial signals is accentuated. Differences between the DW and MOTIVE approaches with ASL include issues related to measurement points, spin-labeling efficiency, ease of implementation, field-strength dependence, accuracy, and RF power deposition, as follows: 1) Only two measurement points (with and without suppression of arterial signals) are obtained in the DW method, while more points at multiple levels of tissue signal intensity are obtainable with MOTIVE. The large dynamic range afforded by multiple MT saturation levels in the MOTIVE method may potentially yield more accurate CBV_a than that obtained with a simpler two-point approach. 2) In the DW gradient approach, ASL RF pulse(s) can be applied during the entire spin preparation time. However, in the MOTIVE method, MT-inducing RF pulses must be inter-

leaved with ASL RF pulses during the spin preparation period, which reduces the spin-labeling efficiency (by 50% in our study). The potential for higher spin-labeling efficiency in the DW method increases the accuracy of CBV_a quantification. 3) Implementation of the DW technique is simple with a one-coil setup for both CASL and pulsed ASL (PASL), and is usable at any MT level. The MOTIVE method with CASL requires modulation of MT levels without changing the ASL efficiency, which is not trivial. However, the MOTIVE approach can be implemented with PASL by the application of variable MT-inducing RF pulses during the spin labeling period (e.g., inversion time in flow-sensitive alternative inversion recovery (FAIR) (33)). 4) High magnetic fields are advantageous for both CBV_a measurement methods due to increased sensitivity. Also, at high field the convergence between transverse relaxation rates of tissue and blood minimizes any error that may result when the difference of relaxation rates is not considered. At 9.4 T, the T_2 values of tissue and arterial blood water are similar, but at low magnetic fields T_2 of arterial blood is longer than that of tissue. Ignoring this relaxation difference will cause an overestimation of v_a: when TE is 40 ms, CBV_a is overestimated by 35% at 1.5 T with arterial blood and tissue T_2 values of 254 ms (34) and 90 ms (35), and by 11% at 4.7 T with arterial blood and tissue T_2 values of 83 ms (27) and 67 ms (28), respectively. This error can easily be minimized by selecting a short TE value; however, a slightly longer TE is needed for insertion of gradient pulses in the DW method as compared to the MOTIVE approach. 5) When CBF is extremely elevated (such as during hypercapnia), the extraction fraction may decrease. An appropriate *b*-value in the DW approach removes labeled arterial blood signals without significantly reducing any unextracted labeled capillary signals. However, in the MOTIVE approach the unextracted labeled capillary spins appear along with arterial blood signals (see Discussion in Ref. 2). At very high flow rates the contribution from unextracted spins can be significant. In this case CBV_a determined by the DW technique may be accurate, but CBV_a determined by the MOTIVE technique will be overestimated. 6) MT-inducing RF pulses in the MOTIVE approach can cause significant power deposition, especially at high magnetic fields, which is unacceptable for human application. The DW-ASL technique can be used to measure CBV_a in animals and humans.

CONCLUSIONS

The source of the pseudo-diffusion component in the IVIM model was examined in ASL studies with the addition of DW gradients, by varying both the post-labeling delay time and the MT levels. Our data suggest that the pseudo-diffusion component in ASL originates from arterial blood. Based on this association, we quantified both CBV_a and CBF by ASL with DW gradients. This technique can be used as a tool to determine the change of CBV_a during increased neural activity, which may provide insights into vascular control mechanisms.

ACKNOWLEDGMENT

We thank Kristy Hendrich for helpful discussion and critical reading of the manuscript.

REFERENCES

1. Rosen BR, Belliveau JW, Vevea JM, Brady TJ. Perfusion imaging with NMR contrast agents. Magn Reson Med 1990;14:249–265.
2. Kim T, Kim SG. Quantification of cerebral arterial blood volume and cerebral blood flow using MRI with modulation of tissue and vessel (MOTIVE) signals. Magn Reson Med 2005;54:333–342.
3. Ito H, Kanno I, Iida H, Hatazawa J, Shimosegawa E, Tamura H, Okudera T. Arterial fraction of cerebral blood volume in humans measured by positron emission tomography. Ann Nucl Med 2001;15:111–116.
4. Balaban RS, Chesnick S, Hedges K, Samaha F, Heineman FW. Magnetization transfer contrast in MR imaging of the heart. Radiology 1991; 180:671–675.
5. Wolff SD, Balaban RS. Magnetization transfer contrast (MTC) and tissue water proton relaxation in vivo. Magn Reson Med 1989;10:135–144.
6. Ye FQ, Mattay VS, Jezzard P, Frank JA, Weinberger DR, McLaughlin AC. Correction for vascular artifacts in cerebral blood flow values measured by using arterial spin tagging techniques. Magn Reson Med 1997;37:226–235.
7. Petersen ET, Lim TC, Golay X. A model-free quantitative arterial spin labeling approach for perfusion MRI. In: Proceedings of the 13th Annual Meeting of ISMRM, Miami Beach, FL, USA, 2005. p 34.
8. Sleigh A, Francis S, Bowtell P, Gowland P. Measurement of transit times and arterial blood volumes using EPISTAR. In: Proceedings of the 10th Annual Meeting of ISMRM, Honolulu, HI, USA, 2002. p 1058.
9. Hoad C, Francis S, Gowland P. Aterial blood volume and blood volume changes measured using ASL in humans. In: Proceedings of the 11th Annual Meeting of ISMRM, Toronto, Canada, 2004. p 1373.
10. Le Bihan D, Breton E, Lallemand D, Aubin ML, Vignaud J, Laval-Jeantet M. Separation of diffusion and perfusion in intravoxel incoherent motion MR imaging. Radiology 1988;168:497–505.
11. Silva AC, Williams DS, Koretsky AP. Evidence for the exchange of arterial spin-labeled water with tissue water in rat brain from diffusion-sensitized measurements of perfusion. Magn Reson Med 1997;38:232–237.
12. Lee SP, Silva AC, Ugurbil K, Kim SG. Diffusion-weighted spin-echo fMRI at 9.4 T: microvascular/tissue contribution to BOLD signal changes. Magn Reson Med 1999;42:919–928.
13. Orrison WW, Lewine JD, Sanders JA, Hartshorne MF. Functional magnetic resonance imaging. Functional brain imaging. St. Louis: Mosby; 1995.
14. Stejskal EO, Tanner JE. Spin diffusion measurements: Spin echoes in the presence of a time-dependent field gradient. J Chem Physics 1965; 42:288–292.
15. Detre JA, Leigh JS, Williams DS, Koretsky AP. Perfusion imaging. Magn Reson Med 1992;23:37–45.
16. Williams DS, Detre JA, Leigh JS, Koretsky AP. Magnetic resonance imaging of perfusion using spin inversion of arterial water. Proc Natl Acad Sci USA 1992;89:212–216.
17. Zhang W, Williams DS, Koretsky AP. Measurement of rat brain perfusion by NMR using spin labeling of arterial water: in vivo determination of the degree of spin labeling. Magn Reson Med 1993;29:416–421.
18. Silva AC, Zhang W, Williams DS, Koretsky AP. Estimation of water extraction fractions in rat brain using magnetic resonance measurement of perfusion with arterial spin labeling. Magn Reson Med 1997;37:58–68.
19. Silva AC, Zhang W, Williams DS, Koretsky AP. Multi-slice MRI of rat brain perfusion during amphetamine stimulation using arterial spin labeling. Magn Reson Med 1995;33:209–214.
20. Conolly S, Nishimura D, Macovski A. A selective adiabatic spin-echo pulse. J Magn Reson 1989;83:324–334.
21. Alsop DC, Detre JA. Reduced transit-time sensitivity in noninvasive magnetic resonance imaging of human cerebral blood flow. J Cereb Blood Flow Metab 1996;16:1236–1249.
22. Neeman M, Freyer JP, Sillerud LO. Pulsed-gradient spin-echo diffusion studies in NMR imaging. Effect of the imaging gradient on the determination of diffusion coefficients. J Magn Reson 1990;90:303–312.
23. Kwong KK, McKinstry RC, Chien D, Crawley AP, Pearlman JD, Rosen BR. CSF-suppressed quantitative single-shot diffusion imaging. Magn Reson Med 1991;21:157–163.
24. Herscovitch P, Raichle ME. What is the correct value for the brain–blood partition coefficient for water? J Cereb Blood Flow Metab 1985; 5:65–69.
25. Barbier EL, Silva AC, Kim SG, Koretsky AP. Perfusion imaging using dynamic arterial spin labeling (DASL). Magn Reson Med 2001;45: 1021–1029.

26. Le Bihan D, Breton E, Lallemand D, Grenier P, Cabanis E, Laval-Jeantet M. MR imaging of intravoxel incoherent motions: application to diffusion and perfusion in neurologic disorders. Radiology 1986;161:401–407.
27. Atalay MK, Reeder SB, Zerhouni EA, Forder JR. Blood oxygenation dependence of T1 and T2 in the isolated, perfused rabbit heart at 4.7T. Magn Reson Med 1995;34:623–627.
28. Okada Y, Hoehn-Berlage M, Bockhorst K, Tolxdorff T, Hossmann KA. Magnetic resonance imaging and regional biochemical analysis of experimental brain tumours in cats. Acta Neurochir Suppl (Wien) 1990; 51:128–130.
29. Cremer JE, Seville MP. Regional brain blood flow, blood volume, and haematocrit values in the adult rat. J Cereb Blood Flow Metab 1983;3: 254–256.
30. Tropres I, Grimault S, Vaeth A, Grillon E, Julien C, Payen JF, Lamalle L, Decorps M. Vessel size imaging. Magn Reson Med 2001;45:397–408.
31. Schwarzbauer C, Morrissey SP, Deichmann R, Hillenbrand C, Syha J, Adolf H, Noth U, Haase A. Quantitative magnetic resonance imaging of capillary water permeability and regional blood volume with an intravascular MR contrast agent. Magn Reson Med 1997;37:769–777.
32. Wang J, Alsop DC, Song HK, Maldjian JA, Tang K, Salvucci AE, Detre JA. Arterial transit time imaging with flow encoding arterial spin tagging (FEAST). Magn Reson Med 2003;50:599–607.
33. Kim SG. Quantification of relative cerebral blood flow change by flow-sensitive alternating inversion recovery (FAIR) technique: application to functional mapping. Magn Reson Med 1995;34:293–301.
34. Barth M, Moser E. Proton NMR relaxation times of human blood samples at 1.5 T and implications for functional MRI. Cell Mol Biol (Noisy-le-Grand) 1997;43:783–791.
35. Breger RK, Rimm AA, Fischer ME, Papke RA, Haughton VM. T1 and T2 measurements on a 1.5-T commercial MR imager. Radiology 1989;171: 273–276.